Orientation of Ligand Field for Dangling Manganese in Photosynthetic Oxygen Evolving Complex of Photosystem II

Hiroyuki Mino[†*] and Hiroki Nagashima[†‡]

[†]Division of Material Science, Graduate School of Science, Nagoya University, Furo-cho, Chikusa-ku, 464-8602, Nagoya, Aichi, Japan.

ABSTRACT: The spin structure in the S_2 state and the crystal structure of the manganese cluster of the oxygen evolving complex of plant photosystem II was combined by the quantitative evaluation of the magnetic anisotropy of the $g = 4$ signal. The g-values of 3.93 and 4.13 were obtained for the $g = 4$ signal in the directions parallel and perpendicular to the membrane normal, respectively. The peak-to-peak separations were 270 and 420 G for the parallel and perpendicular orientations to the membrane, respectively. By comparison with the crystal structure, the z-axis of the zero-field splitting was ascribed to the direction of the dangling Mn connecting water oxygen, Mn4-O(W1), in the manganese cluster. The results give the first experimental evidence that the valence of the dangling Mn is Mn(III) in the S_2 high spin state. We showed the strong exchange coupling of Mn4 to Mn3 was required for g =4.1 spin state in the four spin couplings, estimated as > ~|-30 cm^{-1}|, indicating that the present closed cubane model in QM/MM calculation cannot explain the $g = 4.1$ spin structure. The onsite zero-field splitting of the dangling Mn was evaluated as −2.3 cm^{-1} under the strong antiferromagnetic couplings (-50 cm^{-1}) with the dangling Mn to the cubane frame in the four coupled spin state. From the viewpoint of the arrangement of the Mn valences in the cluster, a closed cubane model is effective, but no large structural deviation from the S_1 state crystal structure.

1.Introduction

Photosynthetic oxygen evolution occurs at the Mn cluster Mn_4CaO_5 in the photosystem II (PS II) protein complex of plants and cyanobacteria [1-3]. The Mn cluster has five different redox states denoted S_n ($n = 0 – 4$), where S_n advances to S_{n+1} state by oxidation. S_4 is the highest overall oxidation state of the cluster, and it immediately reduces to the lowest state S_0, with the evolution of molecular oxygen[4]. Recent advances in X-ray crystallographic techniques have yielded highly resolved structural images of photosystem II[5-7]. The manganese cluster in the S_1 state is a cubic Mn_3CaO_4 motif coordinated to an additional dangling Mn via an oxo bridge. Mn and O in the cubic structure are labelled as Mn1-3 and O1-4, and the dangling Mn and bridging O are labeled as Mn4 and O5, respectively. The dangling Mn4 is also coordinated with two water molecules (W1 and W2), and two O atoms, provided by the surrounding amino acids [7].

In the S_2 state, three kinds of EPR signals can be observed, namely, the $g = 2$ multiline, $g \approx 4.1$, and $g > 4.1$ ($g = 10$ and 6) signals[8-10]. The $g = 10$ and 6 signals were induced by infrared light illumination at 65 K. Upon annealing above 65 K, the $g = 6$ and 10 signals convert to the $g = 2$ multiline signal[8]. The $g \approx 4.1$ and $g = 2$ multiline signals are in equilibrium at 200 K, where the $g \approx 4.1$ signal converts to the $g = 2$ multiline. The spin state of the $g \approx 4.1$ signal has been characterized as the transition of the ±3/2 state at an effective spin $\boldsymbol{S} = 5/2$ [11-12].

Based on QM/MM calculations, two kinds of signals, the $g = 2$ multiline and $g > 4.1$ signals, have been assigned to the isomer of the manganese cluster in the S_2 state, characterized at the position of the O5 oxygen between Mn1 and Mn4 [13-14]. A shorter Mn4-O5 distance, denoted as "open cubane," leads to the g = 2 multiline, and a shorter Mn1-O5 distance, denoted as "closed cubane," leads to g > 4 signals."

The concept of the moving O5 position with the switching of Mn(III) in pentacoordinate provides a reaction model for the oxygen evolving mechanism [14-16]. The valence of manganese in the S_2 state was proposed to be one Mn(III) and three Mn(IV). Mn(III) is considered to be at Mn1 in the multiline signal [14, 17-19], and at Mn4 in the g > 4.1 signal[14]. On the other hand, QM/MM calculations have not been successful for the molecular structure in the case of the $g \approx 4.1$ signal. Besides, recent XRD results show that the closed cubane structure is not detected in the S_2 state [5-6]. Based on these observations, a new QM/MM calculation is proposed, where Mn(III) is at Mn1 in the high spin state[20]. QM/MM calculations have also indicated that the proton arrangements of the Mn cluster easily modify the spin structure. Therefore, experimental evaluations of the position of Mn(III) based on detailed spin structures is

highly required to understand the chemical mechanisms of photosynthetic water oxidation.

In this study, we evaluated the orientations of the zero-field interactions of Mn(III) that lead to anisotropy of the $g \approx 4.1$ signal. Early work showed the anisotropy of the $g \approx 4.1$ signal in the oriented PS II qualitatively[21]. The distorted structure of the Mn cluster [5-7] allowed us to identify the coordinate axes of the Mn ions based on the orientation dependence of the EPR signals. Based on detail analysis, we assigned Mn4 to Mn(III) for the g = 4.1 signal and provided insight into the spin structure.

2.MATERIALS AND METHOD

2.-1. PS II sample preparation.

PS II membranes were prepared from market spinach according to the method described previously[22]. The membranes were suspended in a medium containing 400 mM sucrose, 20 mM NaCl, 0.5 mM EDTA•2Na and 20 mM Mes/NaOH buffer (pH 6.5). The S_2 state membranes were formed under white light illumination (500 W tungsten lamp) for 5 min at 200 K. The S_1 state membranes were obtained by the dark adaptation of the S_2 state membranes for 120 min at 248 K. The membrane-oriented PS II samples were prepared by drying PS II membranes on a plastic sheet under humid nitrogen gas flow for 15 h at 4 °C. The sheet was cut into 2.5 × 25 mm^2 pieces, loaded into an EPR tube, and frozen immediately. The bottom of the EPR tube was covered with glycerol for heat conduction during the measurements. All treatments were performed under dim green light at 4 ºC.

2.-2. EPR measurements.

X-band CW-EPR measurements were carried out using a Bruker E500 EPR spectrometer with a double rectangular resonator (ER 4105DR) and a gas flow temperature control system (ESR900, Oxford Instruments, Oxford, GB). All EPR measurements were performed at 6 K.

2.-3.Spectral simulations.

Spectral simulations were performed by MATLAB R2019a (The Mathworks, Inc).

3. RESULTS

Figure 1 shows the EPR spectra of the oriented PS II membranes at the angles of (a) 0°, (b) 30°, (c) 60°, and (d) 90° of the external magnetic field $\boldsymbol{B_0}$ relative to the membrane normal $\boldsymbol{n}$. Each spectrum was obtained by subtracting the S_1 state signal from the S_2 state signal (Figure S1). The $g \approx 4.1$ signal was shifted upfield at decreasing angles to $\boldsymbol{B_0}$. At 0°, both the signal linewidth and the *g*-value were minimal, consistent with the earlier qualitative work on the anisotropy of the $g \approx 4.1$ signal in oriented PS II[21]. Figure 2 shows the dependence of the *g*-factor and derivative peak positions on PSII angle. The *g*-value is evaluated by the central field positions between the peaks. A minimum *g*-value of 3.93 and maximum *g*-value of 4.13 were obtained at 0° and 90°, respectively. Based on these results, sine curve fitting gave a calculated shift value of 76 G (Figure S2). The peak-to-peak linewidths were 270 G at 0° and 424 G at 90°. The angular dependence for the negative peak position was small.

The g ≈ 4.1 signal is explained by an effective spin $\boldsymbol{S}$ = 5/2 state [11-12]. The spin Hamiltonian is generally expressed as:

$$\mathcal{H} = g\beta \boldsymbol{S}\boldsymbol{B_0} + \sum \boldsymbol{I}\cdot\boldsymbol{A}\cdot\boldsymbol{S} + D\left[\boldsymbol{S_z^2} - \frac{1}{3}S(S+1)\right] + E\,(\boldsymbol{S_x^2} - \boldsymbol{S_y^2}) \quad (1)$$

, where $\boldsymbol{S}$ and $\boldsymbol{I}$ are electron spin and nuclear spin operators, *D* and *E* are the zero-field splitting (ZFS) parameters, *g* is the *g*-factor, $\boldsymbol{A}$ is the hyperfine tensor, and $\boldsymbol{S}$ is the effective spin operator ($\boldsymbol{S_x}$, $\boldsymbol{S_y}$, $\boldsymbol{S_z}$). Spectral simulations have been performed by diagonalization of the 6×6 matrix of the Hamiltonian. The anisotropy of the g ≈ 4 signal is mainly ascribed to the zero-field splitting parameters, *D* and *E*. The $g \approx 4$ signal has been well characterized by the rhombic parameter *E/D* = 0.25 [11-12].

The rhombic parameter *E/D* is sensitive to the resonance magnetic field, while the *D* value is not very sensitive to the resonance position. Figure S3 shows the powder pattern of the $g \approx 4$ signal, where the parameters used are $g = 2$, $D = -0.445$ cm^{-1}, and $E/D = 0.25$ [12]. Linewidth anisotropy arises from hyperfine interaction, and the total linewidth Γ is expressed as:

$$\Gamma = A_\perp - (A_\parallel - A_\perp)\cos^2\theta \quad (2)$$

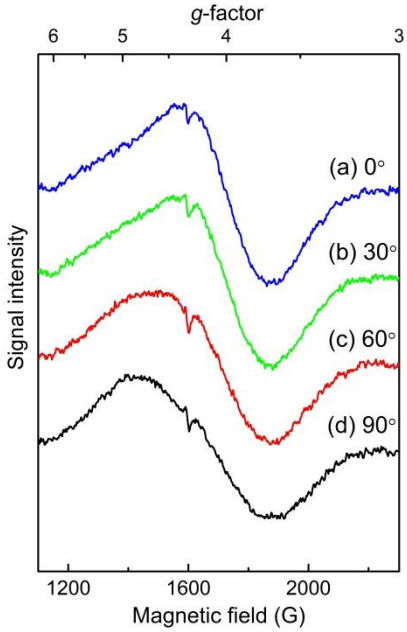

Figure 1: EPR spectra of the $g \approx 4.1$ signals for the oriented PS II membranes at angles of (a) 0°, (b) 30°, (c) 60° and (d) 90° to $\boldsymbol{B_0}$ relative to the membrane normal $\boldsymbol{n}$. Experimental conditions: microwave frequency, 9.67 GHz; microwave power, 4 mW; modulation frequency, 100 kHz; modulation amplitude, 10 G.

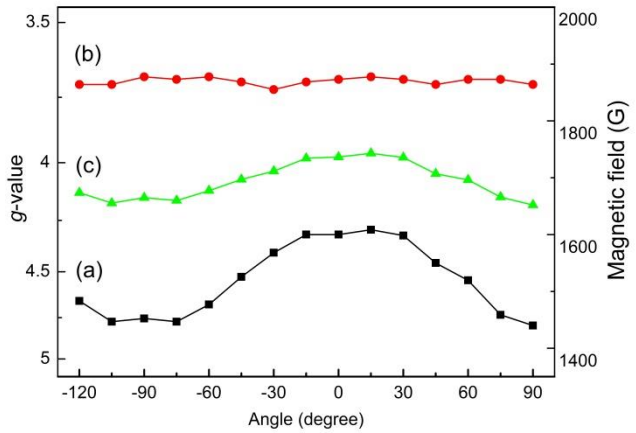

Figure 2: Angular dependence of (a) the positive, (b) negative peak positions and (c) the *g*-value for the g ≈ 4.1 signal.

, where $A_{\parallel}$ and $A_{\perp}$are linewidths at angle θ of the external field $\boldsymbol{B_0}$ to the membrane normal $\boldsymbol{n}$. Linewidths $A_{\parallel}$ and $A_{\perp}$ are assumed Gaussian with 400 and 200 G, respectively. The spectral simulation was performed by diagonalization of the Hamiltonian with the mosaic spread function $G(\theta - \theta_0)$ [22]:

$$G(\theta - \theta_0) = exp\left[-\frac{(\theta-\theta_0)^2}{2\Delta^2}\right] \quad (3)$$

, where θ_0 represents the molecular orientation, defined as zero-field splitting D_Z, relative to the membrane normal vector $\boldsymbol{n}$. Δ is the distribution angle of the mosaic spread, determined as 17°[17, 22].

The difference between the $D_X/D_Y/D_Z$- axes and the axes for Zeeman interaction is ascribed to the molecular orientation. Figure 3 illustrates the possible orientation of the $D_X/D_Y/D_Z$-axes relative to the membrane normal $\boldsymbol{n}$, where the shift of 70 to 80 G was plotted. The results show that the D_Z-direction is located within 30° from the membrane plane. The orientations of the D_X- and D_Y-axes depend on the D_Z-axis. When the D_Z-axis is parallel to the membrane plane, the D_X-axis is 40° from the membrane plane. When the D_X-axis is parallel to the membrane plane, the D_Z-axis is 25° from the membrane plane.

4.DISCUSSION

It is proposed that the zero-field splitting is mainly arises from Mn(III) [14, 23]. In the S_2 state, Mn(III) is proposed to be Mn1 or Mn4[14, 17-18, 23]. The zero-field splitting in the crystalline field consists of each onsite fine structure (d) and interactions between ions. The fine structure Mn(IV) values and dipolar ion-ion interactions are expected to be one order of magnitude smaller than the onsite Mn(III) d value [14, 23]. Therefore, the observed angular dependence is ascribed to Mn(III). In the crystal structure of the S_1 state, Mn4 is hexacoordinated and is surrounded by six oxygen atoms: O4, O5, ASP170, GLU333, and water molecules W1 and W2.

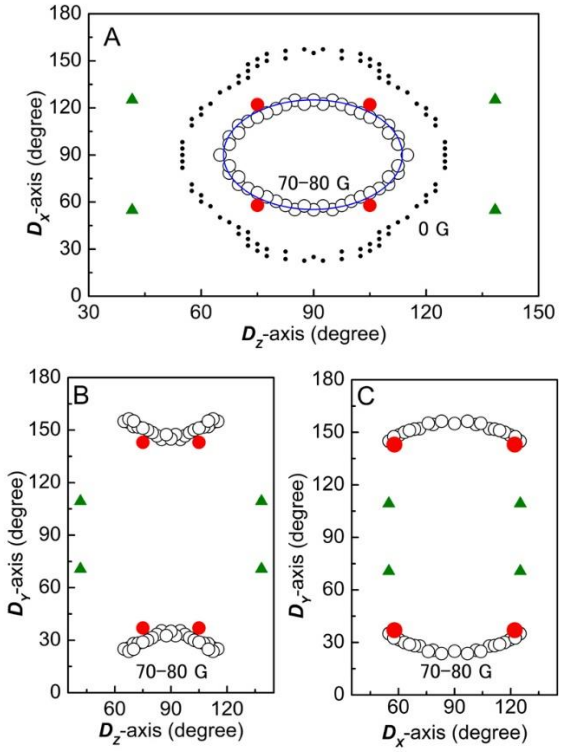

Figure 3. Relationship between the peak shift and the orientation of $D_X/D_Y/D_Z$ -axes relative to the membrane normal $\boldsymbol{n}$ in the oriented PSII. Open circles and dots show the orientations for the calculations corresponding to the 75 ± 5 G shifts and the 0 ± 5 G shifts, respectively. Filled circles (red) show the orientation of the ligand field for Mn4 in the S_1 state crystal structure. Filled triangles (green) show the orientation of the ligand field for Mn1 in the S_1 state crystal structure.

Figure 4 shows the simulated spectra depending on Mn4 molecular axis of the manganese cluster in the crystal structure. The membrane normal $\boldsymbol{n}$ was determined using the locations of the non-heme iron Fe and the reaction center chlorophylls in the crystal structure (PDB ID: 4UB6). The ligand coordinates for Mn4 are distorted from the orthogonal. As the bonding orientations of Mn4-O (W1) and Mn4-O(W2) are close to orthogonal, the Z_0-axis and X_0-axis were defined to the closest directions of Mn4-O (W1) and Mn4-O(W2) with minimal distortions. The Y_0-axis was defined as the axis perpendicular to the X_0- and Z_0-axes. Panel A shows the simulated spectra of the $D_X/D_Y/D_Z$ -axes parallel to (a) $X_0/Y_0/Z_0$ and (b) $Y_0/X_0/Z_0$, and (c) the experimental spectra at the magnetic field angles of 0° and 90°. Panel B shows the simulated spectra of the $D_X/D_Y/D_Z$ -axes parallel to (a) $Z_0/Y_0/X_0$ and (b) $Z_0/X_0/Y_0$. Panel C shows the simulated spectra of the $D_X/D_Y/D_Z$ -axes parallel to (a) $X_0/Z_0/Y_0$ and (b) $Y_0/Z_0/X_0$. In these combinations, only the patterns in panel A show upshifts of field at angle of 0°. The simulated spectra of the $D_X/D_Y/D_Z$ -axes parallel to $X_0/Y_0/Z_0$ (trace a in Panel A) are supported by the experimental spectra within the axis distortion. The filled spheres (red) in Figure 3 show the coordinates for Mn4 in the crystal structure. The results show the Mn4 coordinates in the g ≈ 4.1 signal to be in

close approximation with the S_1 state crystal structure. The result is also consistent with the expected model of D_Z-elongation for Mn(III) [14, 24]. Figure 5 illustrates the orientation of the molecular coordinates and the crystal structure. Mn4-O(W1) is directed to the D_Z-axis, and Mn4-O4 is directed to the D_X-axis. The possible angles for EPR shifts of 70-80 G in the oriented membranes are indicated with the cross marks (light blue). Detail schemes are illustrated in Figure S4.

For comparison, we also examined the case when Mn(III) is located at Mn1. The filled triangles (green) in Figure 3 show the coordinates for Mn1, where, the $X_0/Y_0/Z_0$ -axes are set close to Mn1-O3, Mn1-O1 and Mn1-O5, respectively[24]. The result shows that for a high-spin S_2 state calculated at position Mn1, Mn(III) is not allowed, thus excluding the possibility of a new QM/MM structure for the g=4.1 signal [20]. The scheme is illustrated in Figure S5.

The present results give the first evidence that the valence of the dangling Mn is Mn(III). So far, the valence was suggested by the QM/MM calculations. However, QM/MM calculations were not succeeded for reproducing the high spin structure in the four spin model.

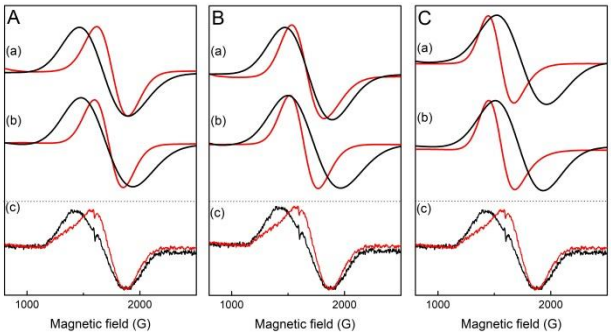

Figure 4. Simulated spectra (a, b) and experimental spectra (c) at angles of 0° (red) and 90° (black). The experimental spectra are the same as those in Fig.2 Panel A: $D_X/D_Y/D_Z$ -axes parallel to (a) $X_0/Y_0/Z_0$ and (b) $Y_0/X_0/Z_0$, Panel B: $D_X/D_Y/D_Z$ -axes parallel to (a) $Z_0/Y_0/X_0$ and (b) $Z_0/X_0/Y_0$, Panel C: $D_X/D_Y/D_Z$ -axes parallel to (a) $X_0/Z_0/Y_0$ and (b) $Y_0/Z_0/X_0$. See text.

Simulations using a four-spin model have also been performed. In the four-spin model, three ferromagnetic coupled Mn unit in a cubane geometry are antiferromagnetic coupled with the dangling Mn4. The ground state $\boldsymbol{S}$ = 5/2 is roughly explained by the antiferromagnetic coupling (J_{eff}) between the cubane frame ($\boldsymbol{S}$ =9/2) and Mn4 ($\boldsymbol{S}$ = 2). In the QM/MM calculation of the closed cubane structure, the exchange interaction between Mn3 and Mn4 was estimated as J_{34} = –7.6 cm^{-1} [14]. The set of J couplings in the QM/MM model corresponded toJ_{eff} = –2.3 cm^{-1} in the two spin model [14]. In the case of the two-spin model, only $|J_{eff}|$ > 10 cm^{-1} was reproducible for the simulation of the g ≈ 4.1 signal [14]. The weak exchange coupling J_{eff} = –2.3 cm^{-1}, upfield shift of the main EPR peak (g = 2 to 3), and additional signals at lower field appears in the small J_{eff} (figure S6), in consistent with the report [14].

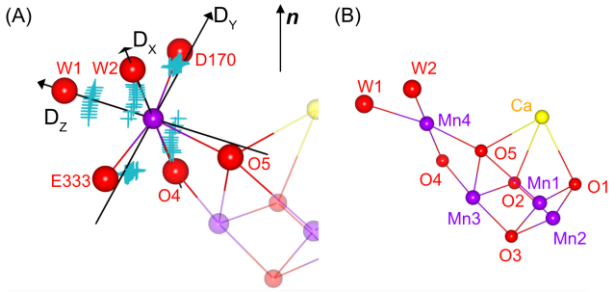

Figure 5. (A) Possible region of orientations of the $D_X/D_Y/D_Z$-axes relative to the crystal structure in the membranes and (B) whole structure of the Mn cluster obtained from the crystal structure (PDB ID: 4UB6). D_X and D_Z axes are set to the closest direction to Mn4-O(W2) and Mn4-O(W1), respectively, corresponding to the filled circles in Fig.3. The possible angles for EPR shifts of 70-80 G in the oriented membranes are indicated by light blue cross marks, corresponded to the open circles in Fig.3. The vector $\boldsymbol{n}$ represents the membrane normal. The red, yellow, and purple balls represent O, Ca and Mn, respectively.

The lower field signals were assigned to the g = 10 and 6 signals [14]. It is notable that the higher field signal around g = 2-3 was not observed experimentally[8]. Therefore, the present QM/MM calculations does not reproduce for neither g=4.1 nor g=6-10 states in the four spin model. In the four-spin model, the magnetic properties were shown to be strongly dependent on the J_{34} between Mn3 and Mn4. Figure S7 shows the resonance field dependence along each axis in the strong coupling model. For the region $|J_{eff}|$ < ~10 cm^{-1}, the energy gap between the ground state and the excited state is estimated to be < ~70 cm^{-1} (7J) in the two-spin model. In the large $|J_{34}|$ region of the four-spin model, estimated as > ~30 cm^{-1}, the g ≈ 4.1 signal was well reproduced using the onsite zero-field splitting of d_4 = –2 to –3 cm^{-1}. Panel C (Figure S7) shows the simulated spectra for the g ≈ 4.1 signal in the oriented membrane using d_4 = –2.3 cm^{-1} in the strong coupling model (J_{34} = –50 cm^{-1}). The orientation of each axis was almost the same as that of the single-spin model, indicating that the orientation dependence is explained by the onsite zero-field splitting of Mn4 for the g ≈ 4.1 signal. In addition, the high energy level of the excited states is required to be isolated from the ground states.

Haddy et al. observed the g = 3.14 and 4.6 signals in Q-band EPR [12]. The g = 3.14 signal was assigned to the ±3/2 transition along the x-axis for $\boldsymbol{S}$ = 5/2. The g = 4.6 signal was tentatively assigned to another transitions within $\boldsymbol{S}$ = 5/2[12]. The onsite zero-field splitting d_4 = –2.3 cm^{-1} was well reproduced for the Q-band spectrum in the strong coupling model (Figure S8).

Dismukes and co-workers have proposed some molecular structures for the S_2 state based on the low valence model[25], which is in disagreement with the high valence model supported by ENDOR[26]. While Dismukes and co-workers suggest a potential misinterpretation of the ENDOR results. One of the low valence structures, Mn (III, IV, IV, II), shows strong cou-

pling of J_{34} = –66.4 cm^{-1} with $\boldsymbol{S}$ = 5/2 ground state. This strong coupling might be preferable for $g \approx 4.1$ signal, but the orientation dependence of the $g \approx 4.1$ signal is not compatible with Mn(III) at the Mn1 position (Fig. 3).

A new QM/MM structure for the S_2 state is reported by Corry and O'Malley without major structural modification from the open cubane state[20]. This is also inconsistent with the results reported here, as Mn(III) is incompatible with the Mn1 position and the exchange couplings are too weak. Recently, Yamaguchi and co-workers have carried out advanced QM/MM calculations and proposed two new closed cubane structures for the S_2 state, with one structure showing that the distance between Mn3-Mn4 is close [27]. As J is very sensitive to the interdistance between spins, the smaller distance between Mn3 and Mn4 might lead to a large J_{34}.

The observable anisotropy in the oriented membranes is sensitive to the orientation of the ligand (Fig.3). Kim et al. have reported the anisotropy of the g ≈ 4.1 signal in ammonia-treated PS II, where a multiline structure was observed in the oriented membrane at 0°[28], ascribed to the reduction of anisotropy. It is proposed that ammonia molecule binds to Mn4, instead of the water molecule [29-30]. The perturbation of the W1 ligand along the D_Z-axis of Mn4 might lead to tilting of the molecular axes.

5. CONCLUSIONS

We determined the orientation of the ligand field for the g ≈ 4.1 signal. The anisotropy of the g ≈ 4.1 signal is caused by the dangling Mn4 in the oxygen-evolving complex of PS II. The onsite zero-field splitting d of Mn(III) is estimated as –2.3 cm^{-1} in the strong coupling model. We showed the strong exchange couplings of Mn4 to Mn3 was required for g =4.1 spin state in the four spin model, and evaluated quantitatively that the strong exchange couplings of Mn4 to Mn3 was estimated as >~|-30 cm^{-1}| From the viewpoint of the arrangement of the valences in the Mn cluster, a cubane model is effective, but no large structural deviation from the S_1 state crystal structure.

ASSOCIATED CONTENT

Supporting Information. **Figure S1**: EPR spectra of g = 4 signals in S_2 state and S_1 state of the oriented PS II membranes; **Figure S2**, The orientation dependence of the g = 4 signal at the angle of the external magnetic field relative to the membrane normal ***n***; **Figure S3**, The simulated spectrum and the energy block diagram for S = 5/2 spin state using the single-spin model; **Figure S4**, The possible orientations of the $D_X/D_Y/D_Z$ axes relative to the Mn4 in the crystal structures; **Figure S5**, Stereo views of the possible orientations of the $D_X/D_Y/D_Z$ axes relative to the ligand fields on Mn1; **Figure S6**, The EPR simulations using the weak coupling model (QM/MM) and the strong coupling models; **Figure S7**, J dependence of the resonant conditions for the strong coupled four spin model; **Figure S8**,(A) The simulated J dependence of the resonant fields in the strong coupled model at Q-band (34 GHz).

AUTHOR INFORMATION

Corresponding Author

*** mino@bio.phys.nagoya-u.ac.jp**

Present Addresses

‡Hiroki Nagashima, Department of Chemistry, Graduate School of Science and Engineering, Saitama University, 255 Shimo-Okubo, Sakura-ku, Saitama 338-8570, Japan

Author Contributions

The manuscript was written through contributions of all authors. / All authors have given approval to the final version of the manuscript.

ACKNOWLEDGMENT

This work was partly supported by a Nanotechnology Platform Program (Molecule and Material Synthesis) of the Ministry of Education, Culture, Sports, Science and Technology (MEXT), Japan.

ABBREVIATIONS

QM/MM, quantum mechanics / molecular mechanics;
EPR, electron paramagnetic resonance; PS II, photosystem II; XRD, X ray diffraction.

REFERENCES

(1) McEvoy, J. P.; Brudvig, G. W. Water-splitting chemistry of photosystem II. *Chem. Rev.* **2006,** *106*, 4455-4483.

(2) Renger, G. *Functional Pattern of Photosystem II*. 2007; Vol. 9, p 237-290.

(3) Lubitz, W.; Chrysina, M.; Cox, N. Water oxidation in photosystem II. *Photosynth. Res.* **2019,**142,105-125.

(4) Kok, B.; Forbush, B.; McGloin, M. Cooperation of Charges in Photosynthetic O_2 Evolution.1. A Linear 4 Step Mechanism. *Photochem. Photobiol.* **1970,** *11*, 457-475.

(5) Kern, J.; Chatterjee, R.; Young, I. D.; Fuller, F. D.; Lassalle, L.; Ibrahim, M.; Gul, S.; Fransson, T.; Brewster, A. S.; Alonso-Mori, R.; Hussein, R.; Zhang, M.; Douthit, L.; de Lichtenberg, C.; Cheah, M. H.; Shevela, D.; Wersig, J.; Seuffert, I.; Sokaras, D.; Pastor, E.; Weninger, C.; Kroll, T.; Sierra, R. G.; Aller, P.; Butryn, A.; Orville, A. M.; Liang, M. N.; Batyuk, A.; Koglin, J. E.; Carbajo, S.; Boutet, S.; Moriarty, N. W.; Holton, J. M.; Dobbek, H.; Adams, P. D.; Bergmann, U.; Sauter, N. K.; Zouni, A.; Messinger, J.; Yano, J.; Yachandra, V. K. Structures of the intermediates of Kok's photosynthetic water oxidation clock. *Nature* **2018,** *563*, 421- 425.

(6) Suga, M.; Akita, F.; Yamashita, K.; Nakajima, Y.; Ueno, G.; Li, H.; Yamane, T.; Hirata, K.; Umena, Y.; Yonekura, S.; Yu, L.-J.; Murakami, H.; Nomura, T.; Kimura, T.; Kubo, M.; Baba, S.; Kumasaka, T.; Tono, K.; Yabashi, M.; Isobe, H.; Yamaguchi, K.; Yamamoto, M.; Ago, H.; Shen, J.-R. An oxyl/oxo mechanism for

oxygen-oxygen coupling in PSII revealed by an x-ray free-electron laser. *Science* **2019,** *366*, 334-338.

(7) Umena, Y.; Kawakami, K.; Shen, J. R.; Kamiya, N. Crystal structure of oxygen-evolving photosystem II at a resolution of 1.9 Å. *Nature* **2011,** *473*, 55-60.

(8) Boussac, A.; Un, S.; Horner, O.; Rutherford, A. W. High-spin states (S ≥ 5/2) of the photosystem II manganese complex. *Biochemistry* **1998,** *37*, 4001-4007.

(9) Casey, J. L.; Sauer, K. Electron-Paramagnetic-Res Detection of a Cryogenically Photogenerated Intermediate in Photosynthetic Oxygen Evolution. *Biochim. Biophys. Acta* **1984,** *767* (1), 21-28.

(10) de Paula, J. C.; Beck, W. F.; Miller, A. F.; Wilson, R. B.; Brudvig, G. W. Studies of the Manganese Site of Photosystem II by Electron Spin Resonance Spectroscopy. *J. Chem. Soc., Faraday Trans. 1* **1987,** *83*, 3635-3651.

(11) Astashkin, A. V.; Kodera, Y.; Kawamori, A. Pulsed Epr Study of Manganese g=4.1 Signal in Plant Photosystem II. *J. Magn. Reson. B.* **1994,** *105*, 113-119.

(12) Haddy, A.; Lakshmi, K. V.; Brudvig, G. W.; Frank, H. A. Q-band EPR of the S_2 state of Photosystem II confirms an S=5/2 origin of the X-band g=4.1 signal. *Biophys. J.* **2004,** *87*, 2885-2896.

(13) Isobe, H.; Shoji, M.; Yamanaka, S.; Mino, H.; Umena, Y.; Kawakami, K.; Kamiya, N.; Shen, J. R.; Yamaguchi, K. Generalized approximate spin projection calculations of effective exchange integrals of the CaMn4O5 cluster in the S_1 and S_3 states of the oxygen evolving complex of photosystem II. *Phys. Chem. Chem. Phys.* **2014,** *16*, 11911-11923.

(14) Pantazis, D. A.; Ames, W.; Cox, N.; Lubitz, W.; Neese, F. Two interconvertible structures that explain the spectroscopic properties of the oxygen-evolving complex of photosystem II in the S_2 state. *Angew. Chem. Int. Ed. Engl.* **2012,** *51*, 9935-9940.

(15) Bovi, D.; Narzi, D.; Guidoni, L. The S_2 State of the Oxygen-Evolving Complex of Photosystem II Explored by QM/MM Dynamics: Spin Surfaces and Metastable States Suggest a Reaction Path Towards the S_3 State. *Angew. Chem., Int. Ed.* **2013,** *52*, 11744-11749.

(16) Chatterjee, R.; Lassalle, L.; Gul, S.; Fuller, F. D.; Young, I. D.; Ibrahim, M.; de Lichtenberg, C.; Cheah, M. H.; Zouni, A.; Messinger, J.; Yachandra, V. K.; Kern, J.; Yano, J. Structural Isomers of the S_2 state in Photosystem II: Do They Exist at Room Temperature and Are They Important for Function? *Physiol. Plantarum.* **2019,** *166*, 60-72.

(17) Asada, M.; Nagashima, H.; Koua, F. H. M.; Shen, J. R.; Kawamori, A.; Mino, H. Electronic structure of S_2 state of the oxygen-evolving complex of photosystem II studied by PELDOR. *Biochim. Biophys. Acta* **2013,** *1827*, 438-445.

(18) Peloquin, J. M.; Campbell, K. A.; Randall, D. W.; Evanchik, M. A.; Pecoraro, V. L.; Armstrong, W. H.; Britt, R. D. ^{55}Mn ENDOR of the S_2 state multiline EPR signal of photosystem II: Implications on the structure of the tetranuclear Mn cluster. *J. Am. Chem. Soc.* **2000,** *122*, 10926-10942.

(19) Stich, T. A.; Yeagle, G. J.; Service, R. J.; Debus, R. J.; Britt, R. D. Ligation of D1-His332 and D1-Asp170 to the Manganese Cluster of Photosystem II from Synechocystis Assessed by Multifrequency Pulse EPR Spectroscopy. *Biochemistry* **2011,** *50*, 7390-7404.

(20) Corry, T. A.; O'Malley, P. J. Proton Isomers Rationalize the High and Low Spin Forms of the S_2 State Intermediate in the Water Oxidising Reaction of Photosystem 2. *J. Phys. Chem. Lett.* **2019**, 10, 5226-5230.

(21) Rutherford, A. W. Orientation of EPR Signals Arising from Components in Photosystem II Membranes. *Biochim. Biophys. Acta* **1985,** *807*, 189-201.

(22) Nagashima, H.; Mino, H. Highly resolved proton matrix ENDOR of oriented photosystem II membranes in the S_2 state. *Biochim. Biophys. Acta* **2013,** *1827*, 1165-1173.

(23) Cox, N.; Ames, W.; Epel, B.; Kulik, L. V.; Rapatskiy, L.; Neese, F.; Messinger, J.; Wieghardt, K.; Lubitz, W. Electronic Structure of a Weakly Antiferromagnetically Coupled $Mn^{II}Mn^{III}$ Model Relevant to Manganese Proteins: A Combined EPR, Mn^{55}-ENDOR, and DFT Study. *Inorg. Chem.* **2011,** *50*, 8238-8251.

(24) Cox, N.; Rapatskiy, L.; Su, J. H.; Pantazis, D. A.; Sugiura, M.; Kulik, L.; Dorlet, P.; Rutherford, A. W.; Neese, F.; Boussac, A.; Lubitz, W.; Messinger, J. Effect of Ca^{2+}/Sr^{2+} Substitution on the Electronic Structure of the Oxygen-Evolving Complex of Photosystem II: A Combined Multifrequency EPR, ^{55}Mn-ENDOR, and DFT Study of the S_2 State. *J. Am. Chem. Soc.* **2011,** *133*, 3635-3648.

(25) Chen, H.; Case, D. A.; Dismukes, G. C. Reconciling Structural and Spectroscopic Fingerprints of the Oxygen-Evolving Complex of Photosystem II: A Computational Study of the S_2 State. *J. Phys. Chem. B* **2018,** *122*, 11868-11882.

(26) Krewald, V.; Retegan, M.; Cox, N.; Messinger, J.; Lubitz, W.; DeBeer, S.; Neese, F.; Pantazis, D. A. Metal oxidation states in biological water splitting. *Chem. Sci.* **2015,** *6*, 1676-1695.

(27) Miyagawa, K.; Isobe, H.; Kawakami, T.; Shoji, M.; Yamanaka, S.; Okumura, M.; Nakajima, T.; Yamaguchi, K. Domain-based local pair natural orbital CCSD(T) calculations of fourteen different S_2 intermediates for water oxidation in the Kok cycle of OEC of PS II. Re-visit to one LS-two HS model for the S_2 state. *Chem. Phys. Lett.* **2019**,734 , 136731.

(28) Kim, D. H.; Britt, R. D.; Klein, M. P.; Sauer, K. The Manganese Site of the Photosynthetic Oxygen-Evolving Complex Probed by EPR Spectroscopy of Oriented Photosystem II Membranes: the g = 4 and g = 2 Multiline Signals. *Biochemistry* **1992,** *31*, 541-547.

(29) Marchiori, D. A.; Oyala, P. H.; Debus, R. J.; Stich, T. A.; Britt, R. D. Structural Effects of Ammonia Binding to the Mn_4CaO_5 Cluster of Photosystem II. *J. Phys. Chem. B* **2018,** *122*, 1588-1599.

(30) Navarro, M. P.; Ames, W. M.; Nilsson, H.; Lohmiller, T.; Pantazis, D. A.; Rapatskiy, L.; Nowaczyk, M. M.; Neese, F.; Boussac, A.; Messinger, J.; Lubitz, W.; Cox, N. Ammonia binding to the oxygen-evolving complex of photosystem II identifies the solvent-exchangeable oxygen bridge (μ-oxo) of the manganese tetramer. *Proc. Natl. Acad. Sci. USA* **2013,** *110*, 15561-15566.

TOC Graphic

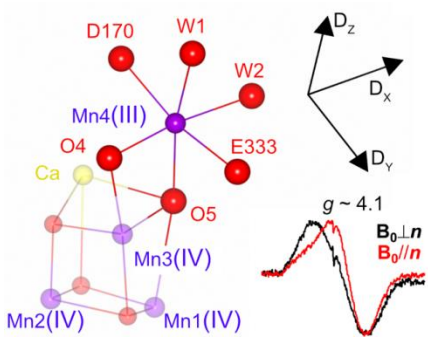
D170
W1
W2
Mn4(III)
O4
E333
Ca
O5
Mn3(IV)
Mn2(IV)
Mn1(IV)
D_Z
D_X
D_Y
g ~ 4.1
B0⊥n
B0//n